

# Machine Learning Integrated with Physical Models for Predicting Flow-Induced Vibration of Tube Bundles

**Authors:** Hu, Dr. Jiachun, He, Dr. Yixiang, Zhang, Dr. Lin, Xu, Dr. Zhiyun, Su, Dr. Yuan, Weiye Zhao, Dai, Prof. Huliang, Prof. Lin Wang, Prof. Huliang Dai

**Date:** 2025-12-02T13:13:00+00:00

## Abstract

Challenges still exist in predicting flow-induced vibrations of tube bundles due to the difficulty in determining fluid forces between tubes. We effectively predict the flow-induced vibrations of tube bundles through a framework that integrates machine learning with physical model. Firstly, a high-fidelity bidirectional FSI model is developed to simulate vibration displacements and fluid forces under various flow conditions. Subsequently, a Long Short-Term Memory (LSTM) network is trained on the FSI-generated time-series data to reconstruct the fluid force field. The trained LSTM model is then coupled with structural dynamics equations. And the iterative solution is conducted to predict system responses under untrained flow velocities. The LSTM model achieves high accuracy in fluid force reconstruction, with a training error below 5%. When generalized to unknown flow conditions, the predictive error for fluid forces remains within 10%. The hybrid LSTM-physical model successfully captures vibration amplitudes across the entire flow velocity spectrum and demonstrates a substantial improvement in computational efficiency compared to traditional FSI simulations. This study establishes a novel model-reconstruction paradigm based on LSTM-physical model for FSI analysis of tube bundles, offering a practical tool for safety assessment and design optimization of tube bundles under flow excitations.

## Full Text

### Preamble

Jiachun Hua#, Yixiang He#, Lin Zhang, Zhiyun Xu, Yuan Su, Weiye Zhao, Huliang Dai\*, Lin Wang

a Department of Engineering Mechanics, Hubei Key Laboratory for Engineering Structural Analysis and Safety Assessment, Huazhong University of Science and Technology, Wuhan 430074, China

b Hanjiang National Laboratory, Wuhan 430010, China

## Abstract

Challenges persist in predicting flow-induced vibrations of tube bundles due to the difficulty in determining inter-tube fluid forces. We address this through a framework that integrates machine learning with physical modeling to effectively predict flow-induced vibrations. First, a high-fidelity bidirectional fluid-structure interaction (FSI) model is developed to simulate vibration displacements and fluid forces across various flow conditions. Subsequently, a Long Short-Term Memory (LSTM) network is trained on FSI-generated time-series data to reconstruct the fluid force field. The trained LSTM model is then coupled with structural dynamics equations, and an iterative solution is performed to predict system responses under untrained flow velocities. The LSTM model achieves high accuracy in fluid force reconstruction, with training error below 5%. When generalized to unknown flow conditions, the predictive error for fluid forces remains within 10%. The hybrid LSTM-physical model successfully captures vibration amplitudes across the entire flow velocity spectrum and demonstrates substantial improvement in computational efficiency compared to traditional FSI simulations. This study establishes a novel model-reconstruction paradigm based on the LSTM-physical model for FSI analysis of tube bundles, offering a practical tool for safety assessment and design optimization under flow excitations.

**Keywords:** Machine learning, FSI, Tube bundles, LSTM-physical model, Hybrid iteration

\*Corresponding author. E-mail address: daihulianglx@hust.edu.cn

# These authors contributed equally to this work

## 1. Introduction

Fluid-structure interaction (FSI) dynamics problems are widely encountered in engineering fields such as aerospace, energy engineering, and marine structures, with the core challenge lying in the complex nonlinear interactions between fluids and structures [1-4]. The tube bundle problem represents a typical FSI scenario [5-6]. Studying FSI dynamics in tube bundles holds significant engineering importance, as it contributes to enhancing the stability and safety of industrial equipment such as heat exchangers and pipeline systems [7-8]. The interaction between fluid and structure directly influences system vibration characteristics, which may lead to fatigue damage or even structural failure, necessitating in-depth investigation of its dynamic behavior.

Current research predominantly employs a combination of numerical simulation

and experimental validation. Examples include three-dimensional numerical models used to verify the coupling effects of fluid viscous damping and structural damping [9], as well as high-fidelity fluid-structure interaction simulation methodologies [10]. Furthermore, advances in unsteady load analysis and FSI simulation techniques have improved understanding of flow-induced instability mechanisms [11-12]. Nevertheless, existing studies still face challenges such as complex boundary conditions, multi-scale effects, and multi-physical coupling issues [13-14]. There remains a need to develop more accurate modeling approaches and experimental methods to address these complexities.

With enhanced computational capabilities and the development of data-driven modeling methods, deep learning-based strategies have gained increasing attention in fluid-structure interaction systems. Deep learning has proven successful in natural language processing [15-17], model reconstruction [18-20], classification and regression [21-23], among other domains. Rooted in the hierarchical architecture of artificial neural networks, deep learning leverages multi-layer non-linear transformations to automatically extract abstract representations from raw data, thereby circumventing the bottleneck of manual feature engineering inherent in conventional machine learning paradigms.

Long Short-Term Memory (LSTM) networks, a prominent deep learning architecture, have revolutionized time series analysis by addressing critical challenges such as long-term dependency modeling and noise resilience. The foundational work of Hochreiter and Schmidhuber [24] introduced the LSTM architecture with memory cells and gating mechanisms, effectively mitigating the vanishing gradient problem in traditional RNNs. This seminal study, cited over 40,000 times, laid the groundwork for sequential data processing. To date, LSTM networks have been widely used in modeling and prediction tasks for complex dynamic systems due to their superior performance in handling time series data. In recent years, researchers have introduced modules such as attention mechanisms and Convolutional Neural Networks (CNNs) to further improve LSTM performance in terms of modeling accuracy and generalization capability [25-27].

Building upon the initial design, researchers quickly began exploring structural variants to optimize performance and efficiency. One significant early improvement was the introduction of peephole connections, which allowed gating units to directly access the cell state, enabling more precise control of information flow (Gers & Schmidhuber [28]). With the resurgence of deep learning, one of the most prominent variants emerged: the Gated Recurrent Unit (GRU). By combining the forget gate and input gate into a single update gate and merging the cell state with the hidden state, GRU significantly reduces model parameters and simplifies computation while achieving performance comparable to standard LSTM across numerous tasks (Cho et al., [29]). LSTM has found applications in diverse fields including speech recognition [30], text summarization [31], and circuit domains [32]. Recent advancements focus on optimizing LSTM architectures and integrating them with other techniques [33-34]. Despite its maturity, ongoing research continues to refine LSTM for larger-scale and more

complex tasks [35-37].

Regarding fluid-structure interaction systems, the significant time dependence of fluid-structure interaction makes LSTM particularly effective for capturing dynamic evolution processes. For instance, in aeroelasticity, Halder et al. [38] constructed a reduced-order model (ROM) based on high-fidelity CFD data using LSTM, successfully predicting gust response and aileron flutter of an airfoil under transonic conditions. This method first compressed data using the Discrete Empirical Interpolation Method (DEIM) before LSTM training, significantly enhancing computational efficiency and prediction accuracy. Furthermore, Zahn et al. [39] applied LSTM to transonic buffet aerodynamic problems, developing an ROM framework capable of capturing self-excited unsteady characteristics. Li et al. [40] proposed an unsteady aerodynamic reduced-order model based on an LSTM network, validated on a NACA 64A010 airfoil across multiple Mach numbers. The model accurately captures both aerodynamic and aeroelastic characteristics while demonstrating significantly higher computational efficiency compared to traditional CFD approaches.

Despite continuous emergence of novel LSTM variants, large-scale empirical studies have systematically compared these architectures. Their findings indicate that while certain variants may exhibit advantages on specific tasks, none consistently and significantly outperforms the standard LSTM architecture across all applications (Greff et al., [35]; Zaremba et al., [41]). This conclusion underscores the robustness and effectiveness of the original LSTM design, while also highlighting that structural innovations tailored to specific problem domains remain crucial for improving model performance.

Based on the wide application of LSTM neural networks in time series analysis, this study combines LSTM with physical modeling to develop an efficient fusion iterative method for predicting vortex-induced vibration of tube bundles. First, the nonlinear mapping relationship between vibration displacement and fluid force in the tube bundle system is established using an LSTM neural network, with model accuracy and generalization verified through training and testing results. Second, fluid forces are obtained through the deep learning model and applied to the structural dynamics equations to solve for system dynamic responses, with results compared against CFD methods in terms of time and efficiency. Finally, based on the LSTM-physical model framework, a fusion iterative solution method is developed for predicting data under unknown parameters, significantly improving prediction efficiency for flow-induced vibration responses. The paper is organized as follows: Section 2 introduces the model and computational method based on the LSTM-physical model; Section 3 presents LSTM model and iterative prediction results; and Section 4 draws conclusions.

## 2.1 Model Description

The research model in this paper is a nine-tube bundle configuration from nuclear engineering evaporative heat exchange, shown in Figure 1. The tube bundle adopts a  $3 \times 3$  square array configuration, as illustrated in Figure 1(b). All tubes are permitted to vibrate in both the in-line ( $x$ ) and cross-flow ( $y$ ) directions. The vibration of each tube influences the entire flow field, thereby affecting the vibrations of other tubes in the bundle. Consequently, the fluid forces acting on the tube bundle depend on the vibration displacements and velocities of each tube. The dynamic model governing the tube array is described by the equations:

$$m_t \ddot{x}_i + c_t \dot{x}_i + k_t x_i = F_t^x, \quad i = 1, 2, \dots, N$$

where  $m$ ,  $c$ , and  $k$  represent the mass, damping, and stiffness of the tubes, respectively.  $F$  denotes the fluid force, the subscript  $i$  indicates the  $i$ -th tube, and  $N$  represents the total number of tubes in the bundle. The physical parameters of the tube bundle are listed in Table 1. The pitch ratio is defined as the center-to-center distance between two adjacent tubes divided by the tube diameter. The natural frequency of the tube  $\omega$  is calculated by  $\sqrt{k/m}$ , and  $c$  is expressed as  $2m\zeta\omega$ , where  $\zeta$  is the damping ratio.

**Table 1.** Physical parameters of the tube and fluid

Parameter	Value
Length	12.6 mm
Tube outer diameter	1.3 mm
Tube wall thickness	0.4 kg/m
Mass per unit length of tube	1.08E11 N/m <sup>2</sup>
Young's modulus	
Pitch-to-diameter ratio	
Damping ratio	

The computational domain is a rectangular region measuring  $40D \times 60D$ , as illustrated in Figure 1(b). The velocity inlet is positioned  $20D$  upstream from the tube bundle region, with a wake region extending  $40D$  downstream. The tube bundle is located  $20D$  from both the upper and lower no-slip boundaries, ensuring negligible boundary effects on tube vibrations. To accurately capture complex flows surrounding the tube bundle and in the wake region, refined meshes are implemented in both the in-line ( $x$ ) and cross-flow ( $y$ ) directions.

## 2.2 Method Framework

Given the high computational cost associated with fluid-structure interaction (FSI) simulations and the powerful nonlinear regression capability of deep learn-

ing, this paper proposes an iterative methodology that integrates FSI with a Long Short-Term Memory (LSTM) deep learning model. The workflow, illustrated in Figure 2 [Figure 2: see original paper], comprises three main modules: data acquisition, deep learning model construction, and a hybrid iterative process.

In fluid mechanics, fluid-structure interaction modeling is characterized by computationally intensive processes that often result in inefficient and costly data acquisition. However, deep learning approaches have demonstrated notable advantages in prediction accuracy and generalization efficiency. Among these, Long Short-Term Memory (LSTM) neural networks are particularly recognized for their capability to capture long-term dependencies in temporal data, outperforming conventional neural networks through their ability to retain information over extended sequences.

To address these challenges, this study proposes an efficient predictive framework for FSI modeling that utilizes an LSTM-based deep learning architecture. The primary objective is to establish a decoupled mapping model between structural vibration displacements and fluid-induced forces. In contrast to direct data-driven prediction models, which are heavily reliant on input data availability under specific conditions, an iterative computational strategy is introduced that progressively generalizes from known training data to untrained flow scenarios. This approach is designed to achieve accurate prediction of both input and output variables under unknown operational conditions using only initially available training data, thereby reducing dependency on additional costly simulations or experiments.

The proposed method employs bidirectional fluid-structure interaction simulations to obtain a limited set of flow-condition data, which are used as training data to train and test an LSTM model. This model achieves accurate predictions on both training and testing sets while effectively capturing temporal dependencies within the sequence data. To enhance its data extrapolation capability despite limited training data, an iterative fusion process is implemented. Starting with known flow conditions as initial values, the LSTM predictions and structural dynamics analysis results are successively updated in a recursive manner until convergence to the target solution is attained. Through this procedure, the method enables effective data supplementation for unknown flow conditions and significantly improves computational efficiency.

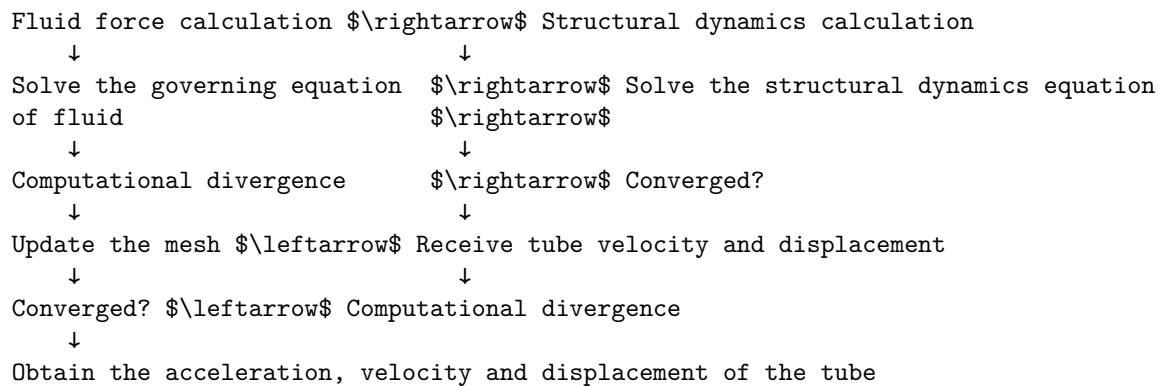
### 2.3 Two-Way FSI Approach

This study employs a two-way fluid-structure interaction approach to generate the training dataset required for the LSTM method. Two-way FSI typically utilizes a partitioned coupling scheme, where the fluid and solid domains are solved separately with iterative data exchange.

For the fluid domain, the CFD solver computes solutions for both the continuity equation and momentum equations. Subsequently, the fluid forces ob-

tained from the CFD solver are imported into the dynamic equations to conduct structural dynamics analysis. An adaptive algorithm is employed to solve the dynamic equations, where each time step is subdivided into multiple substeps for computation. Finally, the displacement, velocity, and acceleration obtained from solving the dynamic equations are transferred to the CFD solver to update the fluid domain mesh. Through this two-way coupling process, the displacement input and fluid force output data are obtained, providing an effective data source for training. However, it should be noted that low computational efficiency and high computational cost are inevitable drawbacks of this method.

**Figure 3** [Figure 3: see original paper] Schematic of two-way FSI approach.



## 2.4 Long Short-Term Memory Neural Network

Structural fluid-structure interaction vibration constitutes a complex dynamical phenomenon, often exhibiting periodic or even chaotic motion with pronounced temporal dependencies. To address such challenges, this study introduces a Long Short-Term Memory (LSTM) neural network for handling time-series problems. Compared to traditional fully connected neural networks (MLP) and standard recurrent neural networks (RNN), the LSTM architecture has garnered significant attention due to its ability to maintain long-term information retention.

The Long Short-Term Memory (LSTM) network is an enhanced variant of recurrent neural networks (RNN), specifically designed to mitigate the vanishing and exploding gradient problems that hinder traditional RNNs in processing long sequences. By incorporating memory cells and gating mechanisms, LSTMs effectively capture and preserve long-range temporal dependencies, leading to superior performance in applications such as time-series forecasting and natural language processing.

At the core of the LSTM lies the memory cell, which facilitates information flow across time steps through a system of gating mechanisms. These gates—comprising the forget gate, input gate, and output gate—collectively regulate the information trajectory. The forget gate determines which information should be discarded from the memory cell, the input gate controls the integration of

new information, and the output gate governs the extent to which the current memory state contributes to the hidden state. This gated structure enables selective retention and propagation of information, making the LSTM particularly adept at modeling long-term dependencies.

At each time step  $t$ , the LSTM computes the activations of the three gates based on the current input  $x_t$  and the previous hidden state  $h_{t-1}$ . First, the forget gate  $f_t$ , governed by a Sigmoid function, identifies portions of the previous cell state  $C_{t-1}$  to be retained. Next, the input gate  $i_t$  and a candidate cell state  $\tilde{C}_t$  collectively determine the content and form of new information to be stored. The updated cell state  $C_t$  is obtained by combining the outputs of the forget gate and the input gate. Finally, the output gate  $o_t$  modulates the extent to which the current cell state  $C_t$  is exposed to the hidden state  $h_t$ .

This process is formally illustrated in Figure 4 [Figure 4: see original paper]:

$$\begin{aligned} f_t &= \sigma(W_f \cdot [h_{t-1}, x_t] + b_f) \\ i_t &= \sigma(W_i \cdot [h_{t-1}, x_t] + b_i) \\ \tilde{C}_t &= \tanh(W_C \cdot [h_{t-1}, x_t] + b_C) \\ C_t &= f_t \cdot C_{t-1} + i_t \cdot \tilde{C}_t \\ o_t &= \sigma(W_o \cdot [h_{t-1}, x_t] + b_o) \\ h_t &= o_t \cdot \tanh(C_t) \end{aligned}$$

In this study, structural displacement is adopted as the input variable, while fluid-induced force is regarded as the output variable. The fluid force at the next time step is predicted based on displacement data from previous time instances, thereby achieving reconstruction of the fluid force model and establishing a mapping relationship between displacement and fluid force. Following the procedure outlined in Figure 3, a loss function is constructed to quantify the similarity between predicted values and ground truth data from the training set. The loss function employed in this work is defined as follows:

$$\mathcal{L} = \frac{1}{N} \sum_{i=1}^N (x_i - \hat{x}_i)^2$$

where  $\hat{x}_i$  represents the predicted value and  $x_i$  represents the actual value.

To enhance the model's ability to extract local features from the data, the dataset is restructured using a sliding window approach. Each window contains a fixed number of consecutive data points, and the data within each window are used to predict the value at the next time step. Prior to this, the dataset is arranged in chronological order to form a continuous long-term time series. Furthermore, to improve training efficiency, the time series dataset is normalized.

In this work, Min-Max normalization is applied to linearly scale the original data into the interval  $[0, 1]$ , as expressed in Equation (8):

$$X_{\text{norm}} = \frac{X - X_{\min}}{X_{\max} - X_{\min}}$$

where  $X$  denotes the original data.

**Figure 4** [Figure 4: see original paper] LSTM architecture diagram.

## 2.5 LSTM-Physical Model and Iteration Method

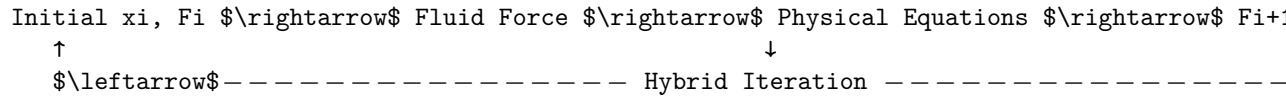
By coupling the LSTM-based fluid force model from Section 2.4 with the physical model, a reduced-order deep learning model referred to as the LSTM-physical model is established for solving structural dynamic responses. The fluid force predicted by the LSTM reduced-order model, denoted as  $F_{\text{LSTM}}$ , is incorporated into the structural dynamics equation (1) of the physical model to drive the vibration simulation, where  $N$  denotes the characteristic dimension of the structural model. The vibration displacement under the corresponding fluid force can thereby be computed, allowing for comparison with original reference data to validate the accuracy of the LSTM-based reduced-order model. It should be noted that the structural dynamics equations of the physical model are solved numerically using a variable-step fourth-order Runge–Kutta method. Since each sub-step is sufficiently small, the fluid force data within any sub-step can be considered consistent with that of the entire macro-step to which it belongs.

Compared to the FSI approach described in Section 2.3, the proposed method eliminates the need for computational fluid dynamics (CFD) simulation, offering significant advantages in both efficiency and computational cost for solving fluid-induced forces. It often requires only minimal prediction and computation time to accurately determine both the fluid force and the structural vibration displacement. Furthermore, in cases where the characteristic dimension  $N > 1$  or vibration occurs in multiple directions, the LSTM-physical framework enables data-driven decoupling of the model, achieving theoretical simplification and model-order reduction, which further enhances predictive efficiency.

However, in typical FSI processes, vibration displacements and fluid forces are inherently coupled, and both are initially unknown for unseen operating conditions prior to analysis. The current LSTM model requires vibration displacement as input to predict the corresponding fluid force, thereby establishing a mapping from displacement to force. A key challenge remains: how can this LSTM model be used to predict both vibration displacement and fluid force under unknown conditions? This prediction must be completed before a full FSI analysis, and this requirement remains an important subject for further research.

Building upon the aforementioned model, this section develops a predictive approach that leverages the generalization capability of the LSTM model, combined with an iterative strategy under the LSTM-physical framework, to rapidly estimate vibration displacements under unknown flow conditions. The overall procedure is illustrated in Figure 5 [Figure 5: see original paper]. Starting from input and output data under known conditions, the fluid force  $F_i$  predicted by the LSTM model is treated as the fluid force term in the governing equations for the target unknown condition. This force is then used in the physical equations to compute the corresponding vibration displacement  $x_{i+1}$ . The newly obtained displacement  $x_{i+1}$  is compared with the previous result  $x_i$ . If the error exceeds a specified tolerance, the updated displacement  $x_{i+1}$  is fed back into the LSTM model to predict a new fluid force  $F_{i+1}$ , and the process is repeated iteratively. Once the error falls within the acceptable range, the result is considered converged, and the final value of  $x_{i+1}$  is taken as the predicted vibration displacement under the unknown flow condition.

**Figure 5 [Figure 5: see original paper]** Based on the iterative approach of LSTM-physical model.



This iterative procedure forms a closed loop integrating the structural dynamics equations and the LSTM model, continuously updating the fluid force and corresponding displacement until convergence is achieved. The method capitalizes on the generalization ability of the LSTM while circumventing its strict dependence on displacement input for fluid force prediction. As a result, it offers significant advantages in extrapolating data under new operational scenarios, even when only limited known data are available.

It should be noted that the proposed method constitutes an iterative framework based on the LSTM-physical model, and its convergence to physically meaningful results depends on a certain level of predictive accuracy from the LSTM model. If the generalization capability of the LSTM is insufficient, the updated displacement  $x_{i+1}$  may fail to approach the true value, potentially leading to divergence in the iterative process. Therefore, the task of data augmentation under limited samples requires a predictive model with adequate accuracy even when trained on small datasets. In this regard, the LSTM architecture holds a natural advantage over traditional multilayer perceptron (MLP) models in handling temporal sequential predictions. Consequently, the iterative strategy presented in this section is closely related to the methods introduced in the preceding three sections. It represents a hybrid iterative methodology that integrates classical structural dynamics with machine learning techniques, offering significant efficiency improvements for solving conventional fluid-structure interaction problems.

### 3. Results

This section presents the results of applying the method proposed in Section 2 to a nine-tube bundle fluid-structure interaction problem. Throughout all training and prediction procedures, the training data were derived from FSI simulation results. The raw data were preprocessed using sliding window segmentation and normalization to generate input and output formats compatible with the LSTM model architecture. The training framework was implemented uniformly in Python 3.7.0 and PyTorch 1.7.0, using an initial learning rate of 0.01 and the Adam optimizer for stochastic gradient descent.

#### 3.1 Data Description

The nine-tube bundle model in this study is illustrated in Section 2.1. The training data consist of time-history records of vibration displacements and fluid-induced forces in both the streamwise ( $x$ ) and transverse ( $y$ ) directions for the nine-tube bundle structure under eight different flow velocities:  $U = 1, 1.5, 2, 2.5, 3, 3.5, 4$ , and  $##$ . The test set comprises corresponding data at  $U = 4.5$ .

**Figure 6 [Figure 6: see original paper]** Dataset of the nine-tube bundle model: (a) input dataset of vibration displacements in the  $x$  and  $y$  directions, (b) output dataset of fluid forces in the  $x$  and  $y$  directions.

As shown in Figure 6(a), the vibration displacement dataset includes multi-channel time series for each tube (numbered 1-9) across the velocity range from 1 to 5. Data corresponding to  $U = 4.5$  are reserved for testing to evaluate the model's generalization capability. Similarly, Figure 6(b) illustrates the fluid force dataset, which also incorporates velocity and tube number as key features. It should be noted that this study focuses particularly on the influence of flow velocity on tube bundle dynamics; hence, velocity is treated as a primary feature of interest. Given the complex distribution of displacements and fluid forces across the velocity domain, the training sample is limited to a small dataset encompassing only the eight specified velocities. The dataset was restructured using a sliding window approach, where each window contains a fixed number of time steps, enabling the use of past data within the window to predict the next time step. Prior to this, the data were sorted in ascending order of flow velocity and normalized to improve training accuracy and facilitate model convergence.

#### 3.2 Model Performance

Separate LSTM models were trained for each directional component: the in-line ( $x$ ) direction and the transverse ( $y$ ) direction. For the in-line ( $x$ ) data, a single-layer LSTM with 64 hidden neurons was employed. The training input consisted of vibration displacement data in the  $x$ -direction, and the output corresponded to fluid forces in the  $x$ -direction. Similarly, for the transverse ( $y$ ) direction, an identical architecture—a single-layer LSTM with 64 hidden neurons—was

used, with y-direction displacement data as input and y-direction fluid forces as output.

**Figure 7 [Figure 7: see original paper]** Data for (a) x and (b) y direction training error curves.

As shown in Figure 7, the training errors for both the x and y directions are presented as functions of training steps. The model at 5500 steps was selected as the reference in-line (x) model for subsequent analysis, while the model at 2500 steps was chosen as the transverse (y) model for further study.

Regarding computational efficiency, the training process required average durations of 2633s and 1560s for data prediction along the x and y directions, respectively. Following training, the prediction time of the model was reduced to approximately tens of seconds. This represents a substantial improvement in temporal efficiency compared to the conventional bidirectional fluid-structure interaction approach, which typically demands an average total computational time of 45 hours. Thus, the conventional bidirectional fluid-structure interaction method requires 32.4 times more computational time than the proposed machine learning approach. The proposed machine learning method demonstrates remarkable advantages in reducing prediction time and associated computational costs.

First, the overall prediction performance on both training and test sets for the two directional components is illustrated in Figure 8 [Figure 8: see original paper]. The figure displays split-violin plots for Tube 7 at each flow velocity, where the left half of each violin represents the true values and the right half corresponds to predictions from the LSTM model. The width of each violin at a given fluid force value  $F$  reflects the probability distribution of that value over the entire time history. The violin corresponding to  $U = 4.5$  represents the test set. Figure 8 also visually conveys the range and trends of the fluid force data.

The training and test data for each velocity consist of time-history records associated with tube identity and flow velocity. By comparing the contours and extremes of the distributions between the true and predicted sides, one can effectively evaluate both local and global prediction accuracy of the model. As shown in Figure 8, the predictive models for both  $F_x$  and  $F_y$  achieve high accuracy on the training set, with predicted distributions and ranges closely matching the ground truth. On the test set, the predictions generally maintain consistent data ranges and exhibit similar distribution shapes compared to the ground truth. However, the overall agreement is slightly weaker than that achieved on the training set. This outcome can be attributed to the limited size of the training dataset, which poses challenges for the model in achieving perfect generalization to untrained conditions.

**Figure 8 [Figure 8: see original paper]** Violin plots comparing predicted and true values on training and test sets: (a) in-line (x) direction for Tube 7, (b) transverse (y) direction for Tube 7.

Secondly, Figure 9 [Figure 9: see original paper] presents time-domain and frequency-domain analysis results of the fluid force predictions generated by the LSTM model, with selected examples provided to further illustrate model accuracy. Given that previous FSI studies have identified lock-in phenomena frequently occurring near flow velocities of  $U = 1.5 - 2$ , particular emphasis is placed on training and prediction performance within this velocity range. The figure displays predicted and simulated time-domain values of fluid force  $F_x$  for Tubes 3, 4, and 7 at flow velocities  $U = 1.5, 2$ , and  $2.5$ . Figures 9(a)–(c) compare predicted and true values across these three tubes under each velocity. In each subfigure, dashed lines represent true values while solid lines denote predictions, showing close agreement in the time domain. Selected frequency-domain results are presented in Figure 9(d), which includes power spectral density curves for the predictions of all three tubes at  $U = 2$ .

The results demonstrate that the LSTM model achieves strong performance in both time and frequency domains, delivering high precision in fluid force analysis compared to full FSI simulations. To further quantify model accuracy, the relative  $L_2$  error and root mean square error (RMSE) are calculated for each tube across the training velocity intervals using the following expressions:

$$\text{Relative } L_2 \text{ Error} = \frac{\|F_{\text{pred}} - F_{\text{true}}\|_2}{\|F_{\text{true}}\|_2} \times 100\%$$

$$\text{RMSE} = \sqrt{\frac{1}{N} \sum_{i=1}^N (F_{\text{pred},i} - F_{\text{true},i})^2}$$

The relative  $L_2$  error and root mean square error (RMSE) corresponding to the results in Figure 9 are summarized in Table 2. The values indicate that the training outcomes fully meet accuracy requirements, with all errors remaining at a very low magnitude.

**Figure 9** [Figure 9: see original paper] Comparison of time-domain and frequency-domain predictions from the LSTM model against FSI results on a subset of the training set: (a) time domain, Tube 3, (b) time domain, Tube 4, (c) time domain, Tube 7, (d) frequency domain at  $U = 2$ .

**Table 2.** Prediction errors on a subset of the training set

Tube number	Velocity $U$	Relative L2 Error, %
3	1.5	2.1
3	2.0	1.8
3	2.5	2.3
4	1.5	1.9
4	2.0	2.0
4	2.5	2.2

Tube number	Velocity $U$	Relative L2 Error, %
7	1.5	1.7
7	2.0	1.9
7	2.5	2.1

Finally, to support subsequent investigations, Figure 10 [Figure 10: see original paper] presents prediction results on a segment of the test set, specifically showing time-domain and frequency-domain performance for Tube 7 at  $U = 4.5$ . Compared to the training set, the test set exhibits a relative  $L_2$  error of 9.90%, which remains within an acceptable range. This indicates that the model is capable of effectively predicting chaotic dynamic behaviors even under untrained flow conditions, demonstrating its validity and reliability. Given that this study is based on a limited sample size—only eight flow velocities—the achieved accuracy on the test set is considered sufficient for follow-up predictive studies. These results can, to a reasonable extent, be regarded as representative of the dynamical response at untrained flow velocities.

**Figure 10** [Figure 10: see original paper] Comparison of time-domain and frequency-domain predictions from the LSTM model against FSI results on a subset of the test set: (a) time domain, (b) frequency domain.

### 3.3 Flow-Induced Vibrations Predicted Through LSTM-Physical Model

This section employs the LSTM model from Section 3.2, integrated with the physical model, to investigate the structural dynamics of the tube bundle following the methodology outlined in Section 2.4. The results presented in Figure 11 [Figure 11: see original paper] correspond to the same operating conditions examined in Figure 9, focusing on three flow velocities near the maximum amplitude and three selected tubes. In Figures 11(a)–(c), solid lines represent time-domain results obtained using the LSTM-physical model for solving tube bundle dynamics, while dashed lines denote results from the full CFD-based FSI method. Figure 11(d) displays a comparison of power spectral densities for Tubes 4, 5, and 7 at  $U = 2$ .

**Figure 11** [Figure 11: see original paper] Comparison of time-domain and frequency-domain predictions between the LSTM-physical model and the FSI reference results: (a) time domain, Tube 3, (b) time domain, Tube 4, (c) time domain, Tube 7, (d) frequency domain at  $U = 2$ .

Both time-domain and frequency-domain analyses demonstrate that the LSTM-physical model achieves high accuracy in capturing the dynamic behavior of the tube bundle. Furthermore, a quantitative evaluation based on relative  $L_2$  error and root mean square error (RMSE), as summarized in Table 3, shows that although the relative  $L_2$  error is slightly higher than that observed during fluid force prediction on the training set, the RMSE of the vibration displacements

obtained through this method is generally an order of magnitude lower than the reference values. This indicates that the proposed approach satisfies the basic accuracy requirements for the intended modeling purpose.

**Table 3.** Prediction errors of vibrational displacement for selected tubes

Tube number	Velocity $U$	Relative L2 Error, %	RMSE
3	1.5	3.2	2.60e-4
3	2.0	2.8	2.03e-4
3	2.5	3.5	1.88e-4
4	1.5	3.0	2.61e-4
4	2.0	3.3	2.78e-4
4	2.5	4.1	5.96e-4
7	1.5	2.9	4.89e-4
7	2.0	3.1	4.82e-4
7	2.5	3.7	4.25e-4

The results presented in this chapter indicate that although the temporal-domain error of the LSTM model is slightly amplified through the physical model-based computational process when predicting vibrational displacements, the frequency-domain results remain highly accurate. More importantly, the proposed model requires significantly less computation time compared to conventional FSI simulations. The outcomes discussed in the preceding two sections validate the accuracy of both the preliminary LSTM model and the integrated LSTM-physical model, thereby establishing a reliable foundation for subsequent hybrid iterative approaches.

While the integration of machine learning with the physical model has partially addressed the challenge of modeling tube bundle dynamics, the analysis of vortex-induced vibrations often focuses on how vibrational displacement amplitudes vary across different flow velocities. It is therefore necessary to extrapolate from limited known velocity data to predict amplitude responses over the entire velocity range of interest. This section employs the previously established model, combined with a hybrid iterative method, to supplement untrained flow conditions with corresponding vibrational responses. It should be emphasized that the vibration displacements predicted in Section 3.2 require fluid force inputs at specific flow velocities. In contrast, the present approach simultaneously predicts both vibrational displacements and fluid forces under unknown flow conditions without requiring any prior data at those velocities.

To enable prediction and supplementation of vibrational displacements at unknown flow velocities using the method described in Section 2.4, it is necessary to incorporate flow-velocity coupling into the fluid force expression. This study achieves this by transforming the original fluid force  $F$  into a product of the flow velocity  $U$  and a modified force term  $f$ , expressed as  $F = g(U) \cdot f$ . The

updated dataset for  $f$  is then used to train the LSTM model, which supports subsequent iterative predictions.

It should be noted that the function  $g(U)$  serves solely to introduce velocity coupling into the fluid force representation. Although the specific form of  $g(U)$  affects the magnitude of the updated  $f$  dataset, it does not alter the fundamental predictive capability of the model. As long as the retrained model achieves prediction accuracy comparable to that obtained with the original dataset, the coupling operation successfully incorporates explicit velocity dependence while preserving model validity. To verify the effectiveness and generality of this coupling approach, two different forms of  $g(U)$ , specifically  $g(U) = U^2$  and  $g(U) = U^{0.25}$ , were tested prior to iterative prediction. This comparison demonstrates that the method remains robust regardless of the specific coupling function chosen.

To experimentally validate the effectiveness of the proposed method, this study focuses on three representative tubes within the nine-tube bundle model: Tube 1, Tube 7, and Tube 8. Tube 1, located at the center, exhibits the most distinctive dynamic behavior. Tube 7, situated in the back row, is minimally influenced by surrounding tubes and serves as an example of relatively isolated structural response. Tube 8, positioned in the front row and directly connected to the center tube, displays dynamic characteristics significantly different from those of the other tubes.

A localized iterative prediction was performed for these three tubes following the velocity-coupling procedure. As shown in Figure 12 [Figure 12: see original paper], the predicted vibrational displacements for Tubes 1, 7, and 8 are presented alongside reference values, with dashed lines indicating predictions and solid lines denoting ground truth. The results demonstrate strong agreement between predicted and actual values. Specifically, the predictions for Tubes 1 and 7 start from the fluid force at  $U = 1.5$  to iteratively supplement the vibrational displacement data at  $U = 1$ , while the prediction for Tube 8 begins with the fluid force at  $U = 2$  to supplement data at  $U = 1.5$ . This localized prediction strategy, incorporating different tubes and various unknown flow velocities, confirms both the effectiveness and generality of the method in extrapolating data for untrained flow conditions.

**Figure 12 [Figure 12: see original paper]** Time-domain and frequency-domain results of data supplementation under unknown conditions for three tubes: (a) time domain, (b) frequency domain.

An analysis is now conducted for two different coupling forms  $g(U)$ . First, for  $g(U) = U^{0.25}$ , Figure 13 Figure 13: see original paper and (d) present the supplemented vibration displacement results across the full velocity range in the x and y directions, respectively. In the figures, orange data points represent vibration displacement data at known flow velocities, while blue points indicate predicted displacement values at unknown velocities obtained using the fused iterative method. The brown shaded region denotes the error band of vibration

amplitudes derived from polynomial fitting based on known data, within which all values are considered highly reliable. The results show that the blue data points, originating from adjacent orange points, yield reasonable predictions of displacement values at intermediate velocities through the fused iterative process. This approach effectively complements the amplitude-velocity curve over the entire range, providing a more complete explanation of vortex-induced vibration behavior of the tube bundle under transverse flow.

For  $g(U) = U^2$ , as shown in Figure 13(a) and (b), the predicted results across the velocity range are also generally satisfactory. However, in high-velocity regimes where the fluid force varies significantly, the quadratic amplification inherent in  $U^2$  magnifies prediction errors substantially, leading to reduced accuracy in these regions. Due to this error amplification effect, the performance of the quadratic coupling form is less robust under high-flow conditions.

Therefore, in subsequent iterative predictions for the tube bundle, the coupling operation with  $g(U) = U^{0.25}$  is adopted, as it proves more effective in achieving accurate and reliable data supplementation across the entire velocity range.

**Figure 13 [Figure 13: see original paper]** Vibration amplitudes in the x and y directions for Tube 1 across flow velocities  $U = 1 - 5$ : (a) x-direction  $g(U) = U^2$ , (b) y-direction  $g(U) = U^2$ , (c) x-direction  $g(U) = U^{0.25}$ , (d) y-direction  $g(U) = U^{0.25}$ .

The same methodology was applied to predict and supplement data for other tubes under unknown flow conditions. Figure 14 [Figure 14: see original paper] presents the results for two additional representative tubes—Tube 7 and Tube 8. Figures 14(a)–(b) and 14(c)–(d) show the variation of vibration amplitudes in the x and y directions, respectively, for Tubes 7 and 8 across the flow velocity range  $U = 1 - 5$ .

It should be noted that the predicted data points remain credible within the error bands. Moreover, the iterative prediction time for each data point on the curve is approximately 10 minutes, demonstrating a substantial temporal advantage compared to the 5 hours required by the fluid-structure interaction method. However, some predictions exhibit noticeable deviations at higher flow velocities. This discrepancy can be primarily attributed to inherent limitations of the LSTM model. In this study, the training data were organized chronologically by increasing flow velocity, forming a multi-segment time series. As a result, data corresponding to higher velocities appear later in the sequence, where the model may struggle with long-term dependencies, leading to gradually accumulating errors toward the end of the sequence.

**Figure 14 [Figure 14: see original paper]** Vibration amplitudes in the x and y directions for Tubes 7 and 8 across flow velocities  $U = 1 - 5$ : (a) x-direction, Tube 7, (b) y-direction, Tube 7, (c) x-direction, Tube 8, (d) y-direction, Tube 8.

Furthermore, the accuracy of the model and the direction of iteration play crit-

ical roles in prediction performance. The current iterative approach relies on a unidirectional LSTM, which leaves room for improvement in terms of predictive precision. Despite these limitations, the hybrid iterative method demonstrates strong generalization capability. It successfully predicts data under untrained conditions using only a limited initial dataset, without requiring additional input during inference. Moreover, it significantly reduces computational time compared to full CFD simulations.

#### 4. Conclusions

In the present work, fluid-structure interaction of a nine-tube bundle model subjected to external cross-flow is studied using a reduced-order modeling framework. The framework integrates a deep time-series LSTM model with a physical model (LSTM-physical model) based on limited training data. A novel iterative method combining this reduced-order model with physical principles was proposed. The prediction framework effectively captures both structural and data-driven features of the tube bundle fluid-structure interaction problem. The deep time-series LSTM model successfully reconstructed the fluid force model for the nine-tube bundle under transverse flow. Additionally, compared to full FSI simulations, the LSTM-physical model and the hybrid iterative method achieved high accuracy with substantially less computational time for predicting structural vibration displacements. The key conclusions are summarized as follows:

1. Compared to highly coupled conventional FSI simulations, the proposed iterative model achieves effective decoupling and enables rapid, efficient predictions. It offers significant advantages in reducing computational cost and improving accuracy, demonstrating broad applicability across various FSI scenarios.
2. Fluid force predictions for various tubes under different flow velocities align closely with FSI results, with relative errors of the reconstructed fluid forces below 5%, and errors for predictions under unknown conditions within 10%. The LSTM-physical reduced-order model accurately predicts nonlinear structural vibration responses, enabling efficient and rapid estimation of FSI-induced displacements.
3. The integrated iterative method incorporating velocity-coupling operations enables simultaneous prediction of both vibration displacements and fluid forces under unknown flow conditions using only data from known velocities. It effectively supplements amplitude responses across the entire velocity range with satisfactory accuracy in both the x- and y-directions, while maintaining computational efficiency far superior to that of FSI-based approaches.

In summary, the LSTM-based iterative method grounded in physical principles offers an efficient solution for FSI analysis of tube bundles. Nevertheless, the predictive accuracy of the deep time-series LSTM model trained on limited data

still has room for improvement. Enhancing the time-series prediction framework will be a primary focus of future work.

## Acknowledgment

This work is supported by the National Natural Science Foundation of China (Nos. 12325201, 12322201 and 12272140), the Open Fund Project of Hanjiang National Laboratory (No. KF2024010), and the Fundamental Research Funds for the Central Universities, HUST (No. 2025JYCXJJ021).

## References

- [1] Qin G Y. 3D wakes on the femtometer scale by supersonic jets[J]. *Nuclear Science and Techniques*, 2023, 34(2): 22.
- [2] Dai H, He Y, Zhou K, et al. Utilization of nonlinear vibrations of soft pipe conveying fluid for driving underwater bio-inspired robot[J]. *Applied Mathematics and Mechanics*, 2022, 43(7): 1109-1124.
- [3] Guo X, Xiao C, Ma H, et al. Improved frequency modeling and solution for parallel liquid-filled pipes considering both fluid-structure interaction and structural coupling[J]. *Applied Mathematics and Mechanics*, 2022, 43(8): 1269-1288.
- [4] Liu K, Yu M, Zhu W. Enhancing wind energy harvesting performance of vertical axis wind turbines with a new hybrid design: A fluid-structure interaction study[J]. *Renewable Energy*, 2019, 140: 912-927.
- [5] Sigrist J F, Broc D. Homogenisation method for the modal analysis of tube bundle with fluid-structure interaction modelling[J]. *Finite Elements in Analysis and Design*, 2008, 44(6-7): 323-333.
- [6] Tan W, Zhao C, Ren P, et al. Fluidelastic instability research of tube bundles by a two-way fluid-structure interaction simulation[J]. *International Journal of Pressure Vessels and Piping*, 2022, 199: 104705.
- [7] Han H, He Y L, Tao W Q, et al. A parameter study of tube bundle heat exchangers for fouling rate reduction[J]. *International journal of heat and mass transfer*, 2014, 72: 210-221.
- [8] Yin G, Ong M C, Zhang P. Numerical investigations of pipe flow downstream a flow conditioner with bundle of tubes[J]. *Engineering Applications of Computational Fluid Mechanics*, 2023, 17(1): e2154850.
- [9] Zhao H, Gao P, Tian R, et al. A three-dimensional refined numerical simulation of cross-flow induced vibration mechanism in the tube bundle[J]. *Nuclear Engineering and Design*, 2023, 405: 112223.
- [10] Brockmeyer L, Merzari E, Solberg J, et al. High fidelity simulation and validation of crossflow through a tube bundle and the onset of vibration[J]. *International Journal of Non-Linear Mechanics*, 2019, 117: 103231.
- [11] Shinde V, Marcel T, Hoarau Y, et al. Numerical simulation of the fluid-structure interaction in a tube array under cross flow at moderate and high Reynolds number[J]. *Journal of Fluids and Structures*, 2014, 47: 99-113.
- [12] Tan W, Zhao C, Ren P, et al. Fluidelastic instability research of tube bundles by a two-way fluid-structure interaction simulation[J]. *International Journal*

- of Pressure Vessels and Piping, 2022, 199: 104705.
- [13] Lai J, Yang S, Tan T, et al. Turbulence-induced vibration of tube bundles subjected to cross-flow and loose support[J]. International Journal of Pressure Vessels and Piping, 2022, 195: 104601.
- [14] Lai J, Tan T, Yang S, et al. Experimental and theoretical study on fluidelastic instability of tube bundles subjected to cross-flow in the parallel direction[J]. Annals of Nuclear Energy, 2022, 169: 108927.
- [15] Li H. Deep learning for natural language processing: advantages and challenges[J]. National Science Review, 2018, 5(1): 24-26.
- [16] Otter D W, Medina J R, Kalita J K. A survey of the usages of deep learning for natural language processing[J]. IEEE transactions on neural networks and learning systems, 2020, 32(2): 604-624.
- [17] Goyal P, Pandey S, Jain K. Deep learning for natural language processing[J]. New York: Apress, 2018: 1624-1633.
- [18] Feng Z Y, Tian J L, Wu T, et al. Unveiling the Re, Cr, and I diffusion in saturated compacted bentonite using machine-learning methods[J]. Nuclear Science and Techniques, 2024, 35(6): 93.
- [19] Shlezinger N, Whang J, Eldar Y C, et al. Model-based deep learning[J]. Proceedings of the IEEE, 2023, 111(5): 465-499.
- [20] Ghommam M, Puzyrev V, Najjar F. Deep learning for simultaneous measurements of pressure and temperature using arch resonators[J]. Applied Mathematical Modelling, 2021, 93: 728-744.
- [21] Ren Y, Zhang L, Suganthan P N. Ensemble classification and regression-recent developments, applications and future directions[J]. IEEE Computational intelligence magazine, 2016, 11(1): 41-53.
- [22] Lakshmanan K, Balatti D, Khodaparast H H, et al. Experimental and numerical gust identification using deep learning models[J]. Applied Mathematical Modelling, 2024, 132: 41-56.
- [23] Mohammadi Foumani N, Miller L, Tan C W, et al. Deep learning for time series classification and extrinsic regression: A current survey[J]. ACM Computing Surveys, 2024, 56(9): 1-45.
- [24] Hochreiter S, Schmidhuber J. Long short-term memory[J]. Neural computation, 1997, 9(8): 1735-1780.
- [25] Lin J, Ma J, Zhu J, et al. Short-term load forecasting based on LSTM networks considering attention mechanism[J]. International Journal of Electrical Power & Energy Systems, 2022, 137: 107818.
- [26] Zha W, Liu Y, Wan Y, et al. Forecasting monthly gas field production based on the CNN-LSTM model[J]. Energy, 2022, 260: 124889.
- [27] Lei Y, Hu J, Ding J. A hybrid model based on deep LSTM for predicting high-dimensional chaotic systems[J]. arXiv preprint arXiv:2002.00799, 2020.
- [28] Gers F A, Schmidhuber J, Cummins F. Learning to forget: Continual prediction with LSTM[J]. Neural computation, 2000, 12(10): 2451-2471.
- [29] Cho K, Van Merriënboer B, Gulcehre C, et al. Learning phrase representations using RNN encoder-decoder for statistical machine translation[J]. arXiv preprint arXiv:1406.1078, 2014.
- [30] Sak H, Senior A W, Beaufays F. Long short-term memory recurrent neural

- network architectures for large scale acoustic modeling[C]//Interspeech. 2014, 2014: 338-342.
- [31] Kumar H, Kumar G, Singh S, et al. Text summarization of articles using lstm and attention-based lstm[M]//Machine Learning and Autonomous Systems: Proceedings of ICMLAS 2021. Singapore: Springer Nature Singapore, 2022: 133-142.
- [32] Çağlayan Y. Development of Resolver Circuit with Long Short Term Memory and Reinforcement Learning Algorithms[C]//Proceedings of International Conference on Advanced Technologies. 2023, 11: 95-99.
- [33] Chen Y, Liu X, Rao M, et al. Explicit speed-integrated LSTM network for non-stationary gearbox vibration representation and fault detection under varying speed conditions[J]. Reliability Engineering & System Safety, 2025, 254: 110596.
- [34] Al-Selwi S M, Hassan M F, Abdulkadir S J, et al. RNN-LSTM: From applications to modeling techniques and beyond—Systematic review[J]. Journal of King Saud University-Computer and Information Sciences, 2024, 36(5): 102068.
- [35] Greff K, Srivastava R K, Koutník J, et al. LSTM: A search space odyssey[J]. IEEE transactions on neural networks and learning systems, 2016, 28(10): 2222-2232.
- [36] Qian Y. English Speech Recognition System Based on Long Short Term Memory Algorithm[C]//2024 6th International Conference on Artificial Intelligence and Computer Applications (ICAICA). IEEE, 2024: 229-233.
- [37] Yuan H, Bi J, Li S, et al. An improved LSTM-based prediction approach for resources and workload in large-scale data centers[J]. IEEE Internet of Things Journal, 2024, 11(12): 22816-22829.
- [38] Halder R, Damodaran M, Khoo B C. Deep learning based reduced order model for airfoil-gust and aeroelastic interaction[J]. AIAA Journal, 2020, 58(10): 4304-4321.
- [39] Zahn R, Winter M, Zieher M, et al. Application of a long short-term memory neural network for modeling transonic buffet aerodynamics[J]. Aerospace Science and Technology, 2021, 113: 106652.
- [40] Li K, Kou J, Zhang W. Deep neural network for unsteady aerodynamic and aeroelastic modeling across multiple Mach numbers[J]. Nonlinear Dynamics, 2019, 96(3): 2157-2177.
- [41] Zaremba W, Sutskever I, Vinyals O. Recurrent neural network regularization[J]. arXiv preprint arXiv:1409.2329, 2014.

*Note: Figure translations are in progress. See original paper for figures.*

*Source: ChinaXiv — Machine translation. Verify with original.*